Integrative Biology

Accepted Manuscript

ROYAL SOCIETY OF CHEMISTRY

www.rsc.org/ibiology

Table of Contents Entry

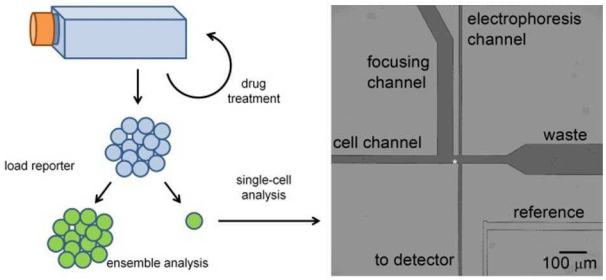

Microfluidic single-cell assays of peptide degradation were performed at varying inhibitor doses, and the resulting data were analyzed by regression modeling to reveal biological effects.

Response of Single Leukemic Cells to Peptidase Inhibitor Therapy Across Time and Dose Using a Microfluidic Device

Michelle L. Kovarik,[1,†] Alexandra J. Dickinson,[1] Pourab Roy,[2] Ranjit A. Poonnen[1], Jason P. Fine,[2] and Nancy L. Allbritton[1,3*]

[1]Department of Chemistry, CB 3290, University of North Carolina, Chapel Hill, NC 27599
[2]Department of Biostatistics, CB 7420, University of North Carolina, Chapel Hill, NC 27599
[3]Department of Biomedical Engineering, University of North Carolina, Chapel Hill, NC 27599 and North Carolina State University, Raleigh, NC 27695

[†]Current affiliation: Department of Chemistry, Trinity College, 300 Summit Street, Hartford, CT 06106

[*]nlallbri@unc.edu

Insight Statement

This work integrates robust microfluidic technology, biochemical assays of individual cells, and regression analysis of the resulting data. The microfluidic device enabled measurement of 100s of individual cells, allowing us to perform a longitudinal study that evaluated the effects of inhibitor dose, reporter peptide loading, and incubation time on the enzymatic degradation of a fluorescent peptide. The heterogeneity of cellular responses to drug treatment was evident both in the number of peptide fragments observed and the rate of peptide degradation and demonstrates the value of single-cell analysis in this area. Additionally, regression modeling of these data revealed changes in peak patterns and degradation rate with increasing dose yielding new insight as to the inhibitor's actions in cells.

Abstract

Single-cell methodologies are revealing cellular heterogeneity in numerous biological processes and pathologies. For example, cancer cells are characterized by substantial heterogeneity in basal signaling and in response to perturbations, such as drug treatment. In this work, we examined the response of 678 individual U937 (human acute myeloid leukemia) cells to an aminopeptidase-inhibiting chemotherapeutic drug (Tosedostat) over the course of 95 days. Using a fluorescent reporter peptide and a microfluidic device, we quantified the rate of reporter degradation as a function of dose. While the single-cell measurements reflected ensemble results, they added a layer of detail by revealing unique degradation patterns and outliers within the larger population. Regression modeling of the data allowed us to quantitatively explore the relationships between reporter loading, incubation time, and drug dose on peptidase activity in individual cells. Incubation time was negatively correlated with the number of peptide fragment peaks observed, while peak area (which was proportional to reporter loading) was positively correlated with both the number of fragment peaks observed and the degradation rate. Notably, a statistically significant change in the number of peaks observed was identified as dose increased from 2 to 4

μM. Similarly, a significant difference in degradation rate as a function of reporter loading was observed for doses ≥ 2 μM compared to the 1 μM dose. These results suggest that additional enzymes may become inhibited at doses > 1 μM and > 2 μM, demonstrating the utility of single-cell data to yield novel biological hypotheses.

Introduction

The importance of cellular heterogeneity in numerous biological phenomena is rapidly being established. In cancer biology, cellular heterogeneity is implicated in formation of the unique tumor microenvironment, drug resistance, and relapse.[1-2] For example, variation in phosphoinositide 3-kinase (PI3K) levels in individual cells regulates a bimodal distribution in AKT activity that affects cell fate.[3] In addition to demonstrating underlying heterogeneity in basal cell signaling activities, recent biological research has also revealed heterogeneity in cellular responses to perturbations. Differences in basal signaling levels can predict the variable drug sensitivity of individual cells,[4] and drug treatment appears to alter the distribution of cells within discrete subpopulations.[5] Importantly, this heterogeneous drug response can contribute to both drug resistance and relapse, as chemotherapeutic drugs select for resistant clones, which may subsequently expand to repopulate the tumor.[6] Indeed, drug treatment has even been proposed as a means to select for tumor initiating cells, so-called cancer stem cells, in the laboratory,[7] and proteomic studies have demonstrated that differential protein expression in response to a drug may be correlated with cell fate, including survival.[8]

While some of these cell-to-cell differences arise from genetic mutations, variability in cellular responses also occurs in genetically identical cells. Local microenvironment, cell cycle, and stochastic fluctuations in mRNA and protein levels all contribute to biological noise that may have substantial effects on cell outcomes.[8-9] For example, malignant cells treated with a mitotic spindle inhibitor exhibited wide variation in drug response, even for cells from the same lineage or subclone.[10] This non-genetic variability in drug response has critical implications for treatment strategies[11] and suggests that direct, single-cell measurements of the activities of targeted enzymes will play an important role in elucidating the range of drug responses possible within a cell population. To date, however, these types of measurements have been limited by low throughput, inadequate robustness, and the challenge of measuring enzyme activities quantitatively and directly.

While a number of established techniques can be used to interrogate individual cells, these methods rarely provide direct readout of the activity of the enzyme or enzymes targeted by a drug. Antibody staining or fluorescent fusion proteins can be used to determine the abundance of an enzyme by microscopy or flow cytometry, and phospho-specific flow cytometry has been used to identify drugs targeting specific pathways.[12] However, these techniques require the availability of suitable antibodies, are affected by nonspecific binding, and do not typically report on enzyme activity directly. Fluorogenic and fluorescence resonance energy transfer (FRET) substrates provide activity readout, but for experiments in intact cells these data are

confounded by the variable and often unknown substrate concentration in each cell. Additionally, fluorogenic and FRET substrates commonly result in a single fluorescent product, regardless of the number of processing steps that might be affected by a drug of interest.[13] Many important cellular processes, including lipid metabolism and peptide degradation, yield numerous potential products from the activity of multiple enzymes.[14-15]

In contrast to fluorogenic or FRET-based substrates, fluorescently-tagged reporter substrates may be modified by multiple enzymes to yield a range of fluorescent products. Both peptide and lipid reporter molecules have been developed for enzymes, including kinases,[14, 16-17] phosphatases,[18] transferases,[19] peptidases,[20-21] and glycosidases.[22-23] Because a fluorescently-labeled reporter substrate and its product forms are not spectrally separated, a physical separation step is necessary to isolate the parent substrate from the resulting product(s) in space or time. Electrophoretic separations, either in a capillary or on a microfluidic device, are well-suited to this application due to their high efficiency and compatibility with low sample volumes. The application of electrophoretic separations to single-cell analysis is termed chemical cytometry. Combined with fluorescent reporter substrates, chemical cytometry provides a direct, quantitative measure of enzyme activity as a function of substrate concentration. These data are obtained by loading an intact cell with a fluorescently-labeled substrate molecule, allowing enzymes in the cell to act on the reporter substrate to yield one or more products, then lysing the cell and separating the contents prior to detection. Early applications of capillary or microfluidic separations of single-cell contents were limited to non-biological analytes (e.g., dyes),[24-26] had limited throughput,[27-29] or analyzed only small numbers of cells.[30-34] Recent technological advancements have addressed these issues, enabling studies of biological analytes such as reporter substrates in hundreds of individual cells.[21, 35-36] The measurement of such large numbers of individual cells allows more sophisticated statistical tools to be applied to these data, revealing novel biological information.

In this work, we apply a microfluidic device for chemical cytometry to studies of peptidase activity in individual drug-treated leukemia cells. Cells were treated with Tosedostat, a non-specific inhibitor with IC50 values in the nanomolar-range for four common aminopeptidases.[37] Cells are dependent on peptidases for protein recycling, and cancer cells are particularly susceptible to inhibition of this process, making Tosedostat and similar drugs promising chemotherapeutics.[38] Consequently, prolonged exposure to Tosedostat represents a significant perturbation to leukemia cells, including the U937 cell line used here. To assess the effect of the drug on enzyme activity, drug-treated cells were assayed both individually and as a population for degradation of a fluorescently-labeled peptide reporter substrate. We used these data to evaluate the affects of drug dose, substrate concentration, and incubation time on the number of fragment peaks observed and the rapidity of peptide breakdown. Notably, the microfluidic platform used here was capable of analyzing tens of cells per hour, and we assayed a total of 678 individual cells over 95 days of continuous drug treatment. Accumulating this quantity of data

allowed us to apply regression models to the single-cell data and to extract biological information and form novel hypotheses using the models.

Experimental Methods

Materials

Extracellular buffer with glucose (ECB-glucose) was composed of 10 mM 4-(2-hydroxyethyl)-1-piperazineethanesulfonic acid (HEPES), 135 mM NaCl, 5 mM KCl, 1 mM $MgCl_2$, 1 mM $CaCl_2$ and 10 mM glucose (pH 7.4). Tris buffer for separations was 25 mM tris(hydroxymethyl)aminomethane (Tris) (pH 8.4). Small unilamellar vesicles were prepared by rehydrating a film of 2 mg egg phosphatidylcholine (Avanti Polar Lipids) in 2 mL of 10 mM Tris and 150 mM NaCl (pH 7.4) with sonification (S-250A, Branson) at a 20% duty cycle for 30 min. The resulting vesicles were stored at 4 °C for at least 2 h and up to 2 weeks prior to use. The reporter peptide, YSYQMALTPVV(K-FAM)TL, was synthesized by Anaspec and stored as a 2 mM stock solution in DMSO at -20 °C under desiccation. Tosedostat (CHR-2797) was obtained from SelleckChem and stored as a 10 mM or 80 mM stock solution in DMSO at -20 °C under desiccation.

Cell culture and treatment

U937 cells were obtained from ATCC and cultured at 37 °C, 5% CO_2 in RPMI media supplemented with 10% fetal bovine serum, 50 μg/mL streptomycin, and 50 units/mL penicillin. Drug-treated media was prepared immediately prior to use by diluting 10 mM or 80 mM Tosedostat in DMSO to the desired final concentration; the stock solution concentration was adjusted to avoid DMSO levels higher than 0.1% in the media. For vehicle control cells, an equivalent volume of DMSO was added to media. Every 3-4 days cells were assayed and passaged to a density of 200,000 cells/mL. The day before assays, cells were resuspended in fresh media at a concentration of 500,000 cells/mL to minimize differences in cell physiology between the vehicle control and drug-treated cells due to cell density, secreted factors, and other attributes.

Viability and proliferation assays

Viability was determined using a trypan blue stain. Cells were pelleted, resuspended in ECB-glucose, and stained for 2-3 min with a final concentration of 0.07% trypan blue. At least 100 cells were counted using a hemacytometer for each viability determination. Proliferation was assessed from cell density and cell cycle assays. Cell density was determined by counting cells with a hemacytometer. For the cell cycle assay, 10^6 cells were washed once in phosphate buffered saline (PBS), then added dropwise to ice-cold 70% ethanol to a final concentration of 200,000/mL. These ethanol-fixed cells were stored at -20 °C for up to 2 months prior to analysis. Cellular DNA was then stained with propidium iodide using the following protocol: cells were resuspended in PBS containing 0.5% BSA, re-pelleted, and suspended in PBS containing 0.1%

Triton X-100, 0.2 mg/mL DNase-free RNase A, and 20 μg/mL propidium iodide at a density of 10^6 cells/mL. Cells were incubated in the staining solution for 15 min at 37 °C, stored on ice for up to 24 h, and filtered through a 40 μm mesh just prior to analysis. The flow cytometer (Beckman-Coulter Dako Cyan ADP) was configured for the 488-nm laser line with the 613/20 emission filter and run on the lowest flow setting. Data were collected in Summit 4.3 software and gated to remove debris and doublets using the propidium iodide signal; a minimum of 10,000 events were collected in gate. The resulting peak area data were analyzed without gating using ModFit LT 4.0 (Verity) to fit the data for debris and aggregates and to determine the percentage of cells in gap (G0/G1), synthesis (S), and mitosis (M) phases using a diploid model.

Microchip fabrication

The SU-8 master was prepared using a silicon wafer and standard photolithography. Briefly, wafers were plasma-cleaned for 20 min (PDC-001, Harrick), spin-coated with SU-8 10 for 30 s at 1500 rpm, and softbaked for 10 min at 95 °C to yield a 25 μm thick layer. The resist was exposed through a chrome photomask (5 μm resolution, Frontline Imaging) to a total dose of 300 μJ using a Karl Suss MA6/BA6 mask aligner. The wafer was then post-exposure baked at 95 °C for 5 min, developed for 2 min in propylene glycol monomethyl ether acetate with gentle agitation, rinsed with isopropanol, and hard-baked for 10 min at 95 °C and 70 min at 120 °C. Hybrid polydimethylsiloxane (PDMS)-glass devices were fabricated using standard procedures.[39] Briefly, a 10:1 mixture of Sylgard 184 prepolymer and curing agent (Dow Corning) was degassed, poured over an SU-8 master, and cured at 100 °C for 15 min. Inlets and outlets were formed at the ends of each channel using a 1-mm biopsy punch. The cured PDMS channels were then permanently bonded to a clean glass coverslip by exposing both pieces to oxygen plasma for 2 min and bringing them into conformal contact. Similarly, reservoirs were cut from siloxane polymer tubing (BioPharm, Masterflex) and plasma-bonded to the channel inlets and outlets. Immediately after device bonding, the channels were filled with a solution of small unilamellar phosphatidylcholine vesicles, which spontaneously fused to form a supported bilayer membrane coating on the channel walls.[40] Assembled, coated devices were stored at 4 °C for no more than 48 hours before use.

Peptide loading

An internal standard (carboxyfluorescein) and the reporter peptide YSYQMALTPVV(K-FAM)TL were loaded into cells by pinocytosis using the Influx reagent kit (Life Technologies). Briefly, 1.1×10^7 cells were pelleted and resuspended in 50 μL of 20 μM carboxyfluorescein and 100 μM peptide in hypertonic loading solution. After 10 min at 37 °C, 10 mL of hypotonic, serum-free media was added to lyse pinosomes and release the carboxyfluorescein and peptide into the cytoplasm. The addition of the hypotonic media was considered t = 0 min and the start of the incubation time for all experiments. Cells were then washed once with complete RPMI media and twice with ECB-glucose. The sample of peptide-loaded cells was then split for ensemble and single-cell assays. For the ensemble samples, 1×10^7 cells were incubated at room temperature at

a density of 1 ×10^6 cells/mL for 1 h, pelleted, resuspended in 20 µL ECB-glucose, and lysed by heating to 95 °C for 4 min. The resulting lysate was centrifuged for 5 min at 4 °C at 14,000 rpm, and the supernatant was collected and stored at -20 °C until analysis. For single-cell analysis, the remaining 10^6 cells were resuspended in ECB-glucose at a concentration of 2 × 10^6 cells/mL.

Single-cell analysis

Single-cell analysis of peptide degradation was performed using a well-characterized device for chemical cytometry.[26, 41] Just prior to use, microfluidic devices for single-cell analysis were flushed for 10 min with filtered, degassed 25 mM Tris buffer (pH 8.4). Peptide-loaded cells in ECB were then added to the sample reservoir and brought to the focal point of a pulsed laser by pressure-driven flow. Firing the pulsed laser resulted in rapid (sub-second) cell lysis, as characterized in earlier work.[42] The released intracellular contents were then drawn electrophoretically into a separation channel running perpendicular to the cell channel, separated with an electric field strength of 500 V/cm, and detected downstream by laser-induced fluorescence. Fluorescence was detected at a photomultiplier tube (7732-01, Hamamatsu), and data were collected at 350 Hz using a current-to-voltage converter (PMT-5, ARI Corp.), hardware filter (10 Hz, Tunable Active Filter 900, Frequency Devices Inc.), and custom LabView software (National Instruments). For comparison purposes, fluorescence values were reported in units of volts since the measured PMT voltage reflected the fluorescence intensity. Data analysis was performed using a custom MatLab program as described previously.[21]

Ensemble sample analysis

Ensemble samples from lysed cells were analyzed by both microchip and capillary electrophoresis (CE). For CE analysis, a commercial instrument (PA-800, Beckman Coulter) was used with a bare 30-cm long, 30-µm i.d. silica capillary. The run buffer was 140 mM borate, 70 mM sodium dodecylsulfate at pH 7.5. The electric field strength was 600 V/cm, and laser-induced fluorescence detection was performed at an effective length of 20 cm. Addition of standards was used to confirm the absence of the parent reporter peptide and to identify the peak co-migrating with free fluorescently labeled lysine (K-FAM). Data were analyzed in OriginPro 8.1 using the multiple peak fit function to fit Gaussian peaks to the electropherograms. A subset of ensemble samples was also analyzed by microchip electrophoresis under conditions similar to those on the chemical cytometry device. Briefly, 20 µm wide, 20 µm deep cross chips were fabricated and coated with a supported bilayer membrane in the manner described above. Chips were flushed with ECB-glucose, and 1 s gated injections were used to dispense ensemble lysate into the separation channel. The lysate samples were then separated with electric field strength of 170 V/cm, and the resulting peaks were detected by laser-induced fluorescence. The fluorescence signal was recorded by a photomultiplier tube (PMT 2000, Advanced Research Instruments Corp.), amplified and filtered as described above, and recorded at 250 Hz by a custom LabView program.

Statistical analysis

Proportional odds models were fit on the number of peaks formed at each dose level. Both an unadjusted model and a model adjusted for time and area were considered. The results of the adjusted model indicated that both time (p-value of 0.036) and area (p-value < 0.001) had significant effects on the number of peaks formed. Hence, the adjusted model was used to draw conclusions about the effect of dose levels on peak formation. To assess factors involved in degradation rate, additional statistical analysis was performed for those cells having 3 fragment peaks. As in our previous work,[21] the first of these 3 fragment peaks was expected to co-migrate with and include K-FAM based on data from ensemble samples, allowing us to use the area of this peak and the incubation time for each cell to determine a proxy value for the rate of degradation. We fit a linear regression model to the log of the average rate proxy value, using the dose level and the total fragment peak area as covariates and assuming that the errors were normally distributed. The total fragment peak area seemed to be an important factor in the rate of peak formation (p-value < 0.001), so it was included in models designed to test the effect of dose on degradation rate. To compare consecutive dose levels, we performed Wald tests,[43] each of which approximately followed a chi-square distribution with 1 degree of freedom under the null distribution.

Results and Discussion

To evaluate the effect of a prolonged chemotherapeutic perturbation on a cell population, we cultured U937 cells, an acute myeloid leukemia cell line, under conditions commonly used to induce drug resistance in other drug-cell line pairs.[44] Cells were cultured for 95 days in the presence of the aminopeptidase-inhibiting drug Tosedostat, and the dose was periodically doubled so that the population was sampled at doses of 1, 2, 4, 8, and 16 μM Tosedostat. During this time, we made ensemble (i.e., population-level) measurements of viability and proliferation and both ensemble and single-cell measurements of peptidase activity (Figure 1, Figure S-1). For assays of peptidase activity, cells were loaded with a fluorescently-labeled peptide reporter substrate. During the incubation period, peptidases in the intact cells processed the peptide reporter to yield fragments. After lysis, the cell contents were separated by electrophoresis, and fluorescent reporter fragments were detected. Previous research has shown that 24 h exposure to media containing 1 μM Tosedostat inhibits degradation of a fluorogenic reporter by 50%,[45] and past work in our laboratory has also demonstrated decreased peptidase activity toward the fluorescent reporter peptide at this dose.[21] In this work, we more thoroughly examined the effect of drug dose on aminopeptidase activity in treated cells.

Single-cell measurements were made using a microfluidic device (Figure 2a) to focus a stream of cells to the focal point of a pulsed laser for lysis (Figure 2b-h), followed by electrophoretic separation of the fluorescently-tagged peptide reporter fragments. We performed a total of 21 single-cell experiments over the course of 95 days and collected data on 678 individual cells (Table S-2). The average duration of data collection was 67 ± 22 min, and we sampled 32 ± 14

cells per experiment at an averaged sustained rate of 30 ± 11 cells/h. This throughput is comparable to our previous work on this system[21] and compares favorably with other microfluidic systems, which have been slower or operated for shorter durations.[27-34] Indeed, the ability to collect chemical cytometry data from large numbers of cells for longitudinal studies is itself an advance, and these data represent an important step forward in single-cell analysis. After analysis, the single-cell data for each dose were pooled to create data sets with 16 to 262 individual cells per dose for further analysis (Table 1).

Variation in number of fragment peaks

Single-cell measurements showed a dramatic change in fragment peak pattern upon drug treatment (Figure 3a). All 43 untreated single cells possessed a single fragment peak, while drug-treated cells possessed fragment peak patterns consisting of 1 to 5 fragment peaks (Figure 3b). Standard solutions of the intact reporter substrate and K-FAM (the fluorescently-labeled amino acid in the reporter) were added to ensemble lysate samples to aid in identifying possible components of the peaks observed. Notably, in all experiments with both untreated and drug-treated cells, the intact reporter peptide was undetected even at the shortest incubation times (< 15 min), suggesting rapid peptidase activity toward the full-length substrate. Because no parent reporter peptide remained at the onset of our experiments, we monitored the fragment peak that co-migrated with the labeled lysine residue as a marker for advanced degradation of the reporter since this represents the smallest detectable fragment. While we cannot rule out co-migration of other fragments with the peak containing the labeled lysine residue, these results and our previous work[21] suggest that in the absence of an inhibitor degradation of the reporter peptide is rapid and complete. In contrast, peptidase activity in drug-treated cells was inhibited relative to a vehicle control at all doses, as evidenced by the presence of additional fragment peaks besides the peak co-migrating with the labeled lysine (Figure 3a).

The number of fragment peaks observed is a simple measure of peptide degradation patterns and can provide useful biological information even in the absence of peak assignments if specific peaks or peak patterns act as biomarkers. For example, we found that although similar fragment peak patterns were observed at each dose, the distribution of these peak patterns shifted with drug dose (Figure 3b). For doses of 1 and 2 μM Tosedostat, the most common peak pattern was 3 peaks. In contrast, at doses of 4 and 8 μM a peak pattern with 2 peaks was observed most frequently.

In further analyzing the relationship between drug dose and the number of peaks observed, we found it necessary to account for variations in the incubation time and reporter substrate concentration between dose groups. Because cells were lysed sequentially as they passed through the microfluidic intersection, individual cells were lysed at random time points. This resulted in a distribution of report substrate incubation times across the population (Figure 4a). Similarly, a distribution of reporter concentrations, measured as total fragment peak area in the electropherogram, was sampled due to variation in loading from cell-to-cell (Figure 4b). This

distribution was skewed toward higher peptide concentrations since lower concentrations were bounded by the detection limit of the system. One-way ANOVA tests showed that the time and peak area distributions were statistically different between some doses ($p = 4.08 \times 10^{-7}$ and $p = 2.27 \times 10^{-5}$, respectively; area values were log-transformed to create a normal distribution). The variation in these distributions arose both from random sampling error and from experimental challenges. For example, the distribution of incubation times for the highest dose, 16 μM, is skewed toward shorter incubation times because these cells were difficult to assay as they did not flow through the device as readily as healthier cells, resulting in shorter experiments.

To evaluate how these factors, along with drug dose, contribute to the number of fragment peaks observed, we constructed a proportional odds regression model (Table S-3). Proportional odds regression estimates the contribution of input variables (e.g., dose, amount of peptide loaded) on an ordinal dependent variable (e.g., peak number).[46] We constructed an adjusted model that examined the relationship between dose and number of peaks observed while including incubation time and total fragment peak area (as a proxy for the amount of peptide in the cell) as explanatory variables in addition to dose (Equation 1):

$$odds(Y \leq j|x) = \exp\left(\alpha_j - \beta_1 x_1 - \beta_2 x_2 - \beta_3 x_3 - \beta_4 x_4 - \beta_5 x_5 - \beta_6 x_6\right) \quad (1)$$

where Y is the number of fragment peaks; x_1 is the incubation time in minutes; x_2 is the total fragment peak area; x_3, x_4, x_5, and x_6 are the indicators for dose levels of 2, 4, 8, and 16 μM, respectively; and each β term is the corresponding coefficient for its variable. The explanatory variables were chosen based on the variation in distributions discussed above; our previous work,[21] which showed a correlation between incubation time and the number of fragment peaks observed; and biochemical intuition that varying substrate concentration and incubation time will affect the number of fragments observed. Indeed, the adjusted model showed that both incubation time and amount of substrate loaded were significant contributors to the number of peaks observed ($p = 0.036$ and $p < 0.001$, respectively). Longer incubation times were associated with smaller numbers of peaks while larger peak areas corresponded to larger numbers of peaks (as evidenced by the negative and positive coefficients, respectively, Table 2). Both effects are explicable in terms of the biological system. During the incubation time, degradation of the peptide is proceeding toward individual amino acids. Because only one amino acid is labeled, the most complete degradation that can be detected is a single fragment peak containing the labeled lysine residue. Longer incubation times result in fragment patterns that are further along this pathway toward a single fragment peak. In contrast, larger peak areas indicate larger quantities of substrate within the cell. For cells measured at identical incubation times, the cell with the highest substrate loading is expected to have less complete degradation, resulting in a larger number of possible fragment peaks.

We also performed Wald tests to determine whether peak patterns for the consecutive dose levels were significantly different or not (Table S-4) and found that the number of peaks observed was similar for the 1 and 2 μM doses ($p = 0.90$). It was also similar for the 4, 8, and 16 μM doses ($p \geq$

0.39 for all consecutive dose pairs). However, the distribution of peak numbers varied considerably when we compared peak numbers observed for 1 μM and 2 μM doses with those for doses of 4, 8, and 16 μM ($p < 0.01$). This change in the distribution of peak patterns may be due to a change in the mode of action of the drug as dose increased from 2 μM to 4 μM. For example, additional aminopeptidases that remain active at low doses may be inhibited at drug concentrations ≥ 4 μM. *In vitro*, the active form of Tosedostat inhibits four common aminopeptidases – LTA_4 hydrolase, leucine aminopeptidase, purine-sensitive aminopeptidase (PuSA), and aminopeptidase N (CD 13) – with IC50 values in the nanomolar range. However, additional aminopeptidases, including aminopeptidase B, puromycin insensitive leucine aminopeptidase (PILSAP), and methionine aminopeptidase-2 (MetAP-2) are inhibited as the dose increases. Tosedostat is a cell-permeable ester but is converted to the active, membrane-impermeant acid form by esterases in intact cells.[37] As a result, quantitative comparisons of published *in vitro* IC50 values and patient serum levels with the drug concentrations in our study are challenging since the concentration of drug in the culture media may differ from intracellular concentrations. However, we expect qualitative changes the distribution of fragments produced as additional enzymes are inhibited, resulting in differences in the number of fragment peaks observed. In this way, changes in peak number distributions – in these experiments or comparable experiments with other reporter substrates – could be a readily observed indicator of inhibition (or activation) of new enzymatic reactions or pathways upon treatment.

To complement this single-cell data, we performed microchip separations on a subset of ensemble samples using conditions similar to the chemical cytometry device (separations run in ECB buffer in phosphatidylcholine bilayer-coated channels). These electropherograms routinely showed four or more peaks for ensemble lysates (Figure 5), even for samples collected at higher drug doses in which the most common peak pattern for single cells was only two fragment peaks. Similarly, higher efficiency separations of the ensemble lysates, conducted on a commercial capillary electrophoresis system, showed as many as 8 fluorescent fragment peaks from drug-treated cells (Figure S-2a). In such ensemble measurements of cell lysates, all detectable peaks will appear in the electropherograms, irrespective of their presence or absence in individual cells. As a result, the number of peaks observed in ensemble lysate samples may be larger than for single cells if the fragment peaks observed in ensemble samples never occur simultaneously in any one cell. These results demonstrate how even simple measures such as fragment peak number benefit from the additional information obtained by single-cell analysis. Changes in observed peak numbers with dose may still manifest themselves in ensemble data as changes in the relative area of specific peaks. However, in the ensemble data, changes in relative abundance of individual peaks present in every cell cannot be distinguished from changes in the number of peaks present in individual cells.

Variation in degradation rate

In our previous work, we determined that in electropherograms containing three fragment peaks, the first fragment peak co-migrated with the labeled lysine residue (K-FAM).[21] The ability to identify this peak allowed us to calculate a proxy measure for the rate of K-FAM formation in individual cells (with three fragment peaks) by dividing the area of the first fragment peak by the incubation time. We expect the resulting value to be proportionate to the rate of formation of K-FAM. For untreated cells, a comparable average rate proxy cannot be calculated because no cells with three fragment peaks were observed; however, we can estimate a lower limit for the average average rate proxy since the single fragment peak observed for these cells also co-migrated with K-FAM. Untreated cells had a median rate of 0.209 V*s/min for the area of the single fragment peak divided by the incubation time. In contrast, cells treated with 1 μM Tosedostat had a median value of 0.087 V*s/min for this average rate proxy. Based on calibration curves for the instrument obtained with a K-FAM standard, these values roughly correspond to rates of formation of 0.4 amol/min and 0.2 amol/min, respectively. Cells treated with higher doses of Tosedostat yielded even lower values for this average degradation rate proxy (Figure 6a, data for 16 μM were omitted because only 3 cells had 3 fragment peaks). For all four drug doses, the distribution of the rate proxies had long tails toward higher values. This tailing occurred because although the majority of the cells had lower degradation rates than the mean, a small number of outlying cells possessed rates that were well-above the average. In an ensemble measurement, these cells would shift the mean observed rate (or average rate proxy) to higher values, as evident from the mean value in the box plots (open squares). Single-cell resolution is required to identify these outlying cells within the population.

One possible explanation for cells with particularly high rates of reporter degradation is that these cells contain proportionately high concentrations of reporter. Indeed, we observe a roughly linear relationship between average rate proxy and total fragment peak area (as a proxy for amount of peptide loaded) (Figure 6b, Figure S-3). The linear relationship between these variables has been observed previously in single-cell measures of peptide degradation[15, 20-21] and suggests first-order kinetics. To quantitatively evaluate drug dose and total fragment peak area as explanatory variables for the average rate proxy, we constructed a multivariate linear model using (Equation 2, Table S-5). To satisfy the assumptions of the linear model, we used the log of the average rate proxy as the dependent variable (Figure S-4) in Equation 2:

$$\log(Y) = \beta_0 + \beta_1 x_1 + \beta_2 x_2 + \beta_3 x_3 + \beta_4 x_4 + \epsilon \quad (2)$$

where Y is the average rate proxy; β_0 is the intercept; β_1 is the coefficient for total peak area; x_1 is the total peak area; x_2, x_3, and x_4 are indicators for dose levels of 2, 4, or 8 μM, respectively; β_2, β_3, and β_4 are the corresponding coefficients; and ϵ is $N(0, \sigma^2)$ for some variance, σ^2. Results from this model indicated that total fragment peak area was a significant factor in determining the average rate proxy ($p < 0.01$) with a unit increase in peak area corresponding to a 2% increase in the average rate proxy (Table 3). Based on calibration data for K-FAM on a similar microchip device, this corresponds to a 2% increase in degradation rate for a 2-amol increase in

peptide loading. The partial R^2 value of 0.37 similarly indicates a strong relationship between the average rate proxy and total fragment peak area; 37% of the variation in average rate proxy was explained by variation in peak area after correcting for the effect of dose.

Data from ensemble lysate samples complemented these single-cell results. For ensemble lysate prepared from cells cultured for 24 h in media with 1 μM drug, capillary electrophoresis results indicated that the labeled lysine containing peak represented ~40% of the total peak area, compared to 100% in the untreated samples (Figure S-2b). Prolonged exposure to this dose and higher doses further decreased the relative peak area of the labeled lysine peak, suggesting enhanced inhibition of aminopeptidases at treatments > 24 h and > 1 μM. Notably, we did not observe substantial increases in the area of the K-FAM containing fragment peak with prolonged exposure to a fixed dose. While moderately higher peak areas were observed for two samples at 4 μM, this increase in K-FAM containing peak area was not accompanied by increased viability or proliferation (Figure S-1), suggesting that wide-spread drug resistance did not emerge in the population on the time-scale of this experiment. The time scale over which drug resistance emerges can vary from weeks to months or longer depending on the drug and cell line.[44] Tosedostat-resistant U937 cells have not been reported in the literature and may require longer than the 95-day duration of these experiments to develop.

The model also suggested a strong relationship between dose and degradation rate after correction for peptide loading (i.e., total fragment peak area) with a partial R^2 value of 0.21. A Wald test showed no significant difference between best fit lines for the higher doses (2-8 μM, $p \geq 0.19$); however, there was a significant difference between regression line for the 1 μM dose and these higher doses ($p < 0.01$). A potential explanation of these results may be that an enzyme involved in formation of the free lysine residue becomes inhibited as the dose increases from 1 to 2 μM, while higher doses may not directly affect any key enzymes in this process. While this explanation is quite speculative, it highlights the potential for regression modeling of single-cell data to generate new hypotheses and avenues of investigation.

Conclusions

We have used microfluidic chemical cytometry to explore heterogeneity in cellular response to varying doses of a chemotherapeutic drug with single-cell resolution. While the single-cell results were in line with ensemble measurements, they also revealed the presence of outlying cells within the population. In the future, this method could be used to detect subpopulations of cells that respond differently to drug treatment. For example, low abundance populations of drug resistant cells could potentially be detected before long-term drug treatment selects for and expands these populations. More broadly, the technology used here could be used to assay changes in the activity of many different enzymes as a function of time and/or external perturbations. To reach its full potential this technology requires the ongoing development of new reporter substrates and suitable separation conditions to resolve these substrates from potential products.

This work also demonstrates that microfluidic chemical cytometry is now sufficiently robust to perform long-term experiments and to generate data for large numbers of cells. As this technology continues to mature, larger sample sizes, higher throughput, and a greater variety of analytes will be possible. The ability to collect data for hundreds of cells across a range of experimental parameters coupled with regression modeling allows detailed analysis of the interactions between drug dose, substrate concentration, analysis time, and cellular heterogeneity. We found positive correlation between reporter concentration and both the number of fragment peaks observed and the rate of peptide degradation. In contrast, incubation time was negatively correlated with the number of peaks observed. As large single-cell data sets are combined with statistical modeling, new biological insights will be revealed and hypotheses generated.

Acknowledgments

The authors thank the UNC Flow Cytometry Core Facility for assistance with flow experiments; Pavak K. Shah for the development of custom data analysis software; and Paul M. Armistead for helpful discussions. This work was supported by grants EB11763 (NLA), CA171631 (AJD), and 1UL1TR001111 (PR and JPF) from the National Institutes of Health.

Electronic Supplementary Information (ESI) available: Viability and proliferation data over the course of the 95 days of data collection; microchannel dimensions; detailed log of single-cell experiments; full results of the unadjusted and adjusted regression models; *p*-values for all pair-wise Wald tests of consecutive dose levels

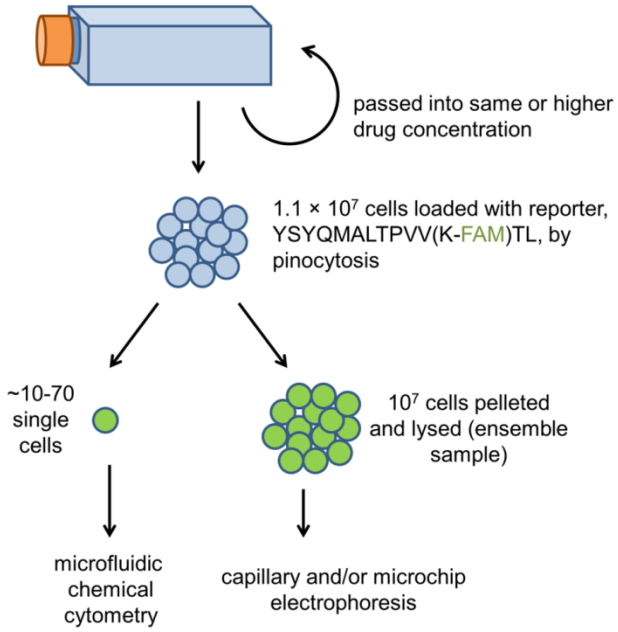

Figure 1. Flow diagram of experimental procedure. Cells were assayed as shown every 3-4 days for 95 days.

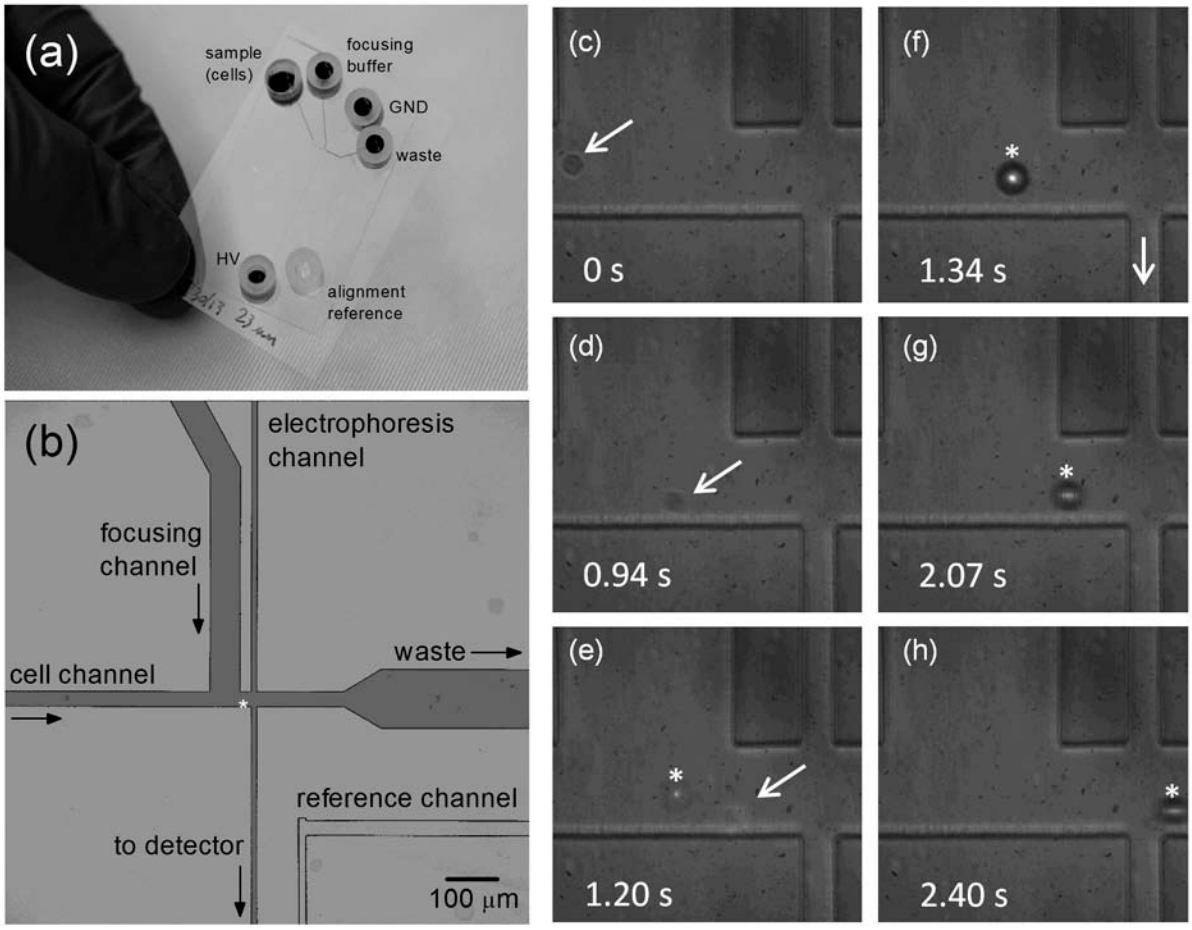

Figure 2. (a) Photograph and (b) schematic of the device used for single cell analysis. (c-d) Pressure-driven flow was used to bring cells to the intersection and to direct them to the focal point (* in (b)) of a pulsed laser for lysis (e). An electric field was applied to the separation channel which effected electrophoretic loading and separation of negatively charged cell contents, including the internal standard and peptide reporter, after lysis. (f-h) Cell debris and the cavitation bubble (*) resulting from lysis were transported by pressure-driven flow to a waste outlet. For (a-b) the channels (except the reference channel) were filled with a trypan blue solution to provide contrast. Dimensions of the channels are given in Table S-1.

Table 1. Summary of single-cell assays performed. Detailed information about the number of cells assayed on each day and the duration of each experiment is given in Table S-2.

Dose (μM)	Days	Number of Single Cells Assayed
0	0	43
1	1-25	262
2	26-68	211
4	69-78	79
8	79-93	68
16	94-109	15

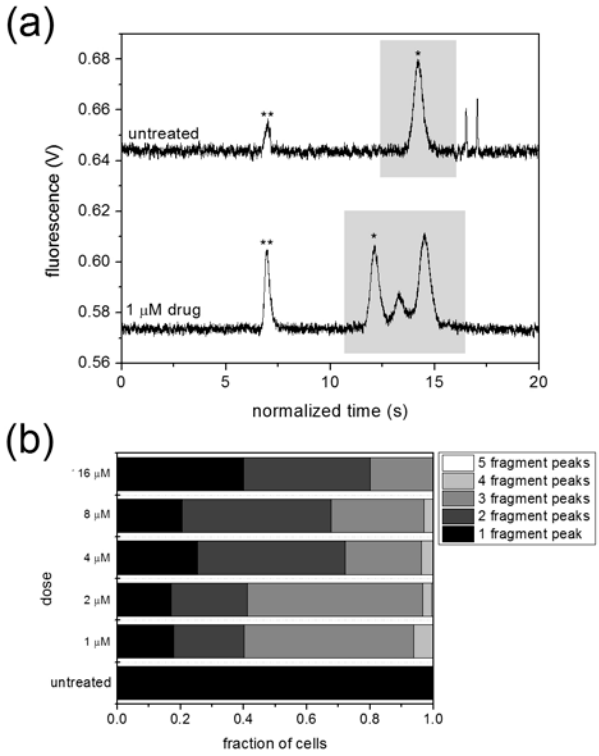

Figure 3. (a) Representative electropherograms from cells with different fragment peak patterns. Each trace is the signal from a single cell. Peaks corresponding to fragments of the reporter peptide are highlighted in gray. The peaks for the internal standard, carboxyfluorescein (**), and the labeled lysine (*) were identified by standard addition to ensemble lysate samples separated under similar conditions (see Figure 5). Differences in migration times were observed from device-to-device, and the *x*-axis for the 1 μM dose sample has been normalized to the migration time of the carboxyfluorescein peak in the untreated sample. The narrow peaks in the electropherogram for the untreated cells are noise from cellular debris in the separation channel. (b) The distribution of fragment peak patterns at each dose.

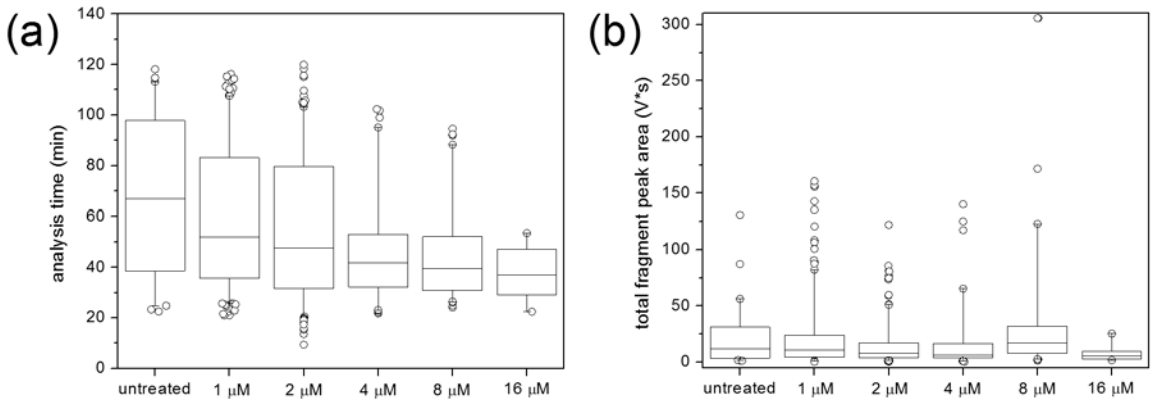

Figure 4. (a) The distribution of cells sampled across time, where $t = 0$ is the application of hypotonic media, which releases the reporter peptide from pinosomes into the cytoplasm. (b) The distribution of total peak areas detected for each cell. Total fragment peak area is proportional to the amount of peptide loaded, i.e. substrate concentration. For both plots, boxes enclose the 25th to 75th percentiles, whiskers indicate 5th to 95th percentiles, and outliers are shown as individual points. The number of individual cells in each group is given in Table 1.

Table 2. Results of the adjusted proportional odds model for peak number. The estimated coefficient for each term indicates how a given variable influences the probability of observing a given number of peaks. For example, the coefficient 0.006 for the effect of time in the adjusted model means that for a unit increase in time (1 min), the log of the odds of occurrence of a single fragment peak (as compared to 2, 3, 4, or 5 fragment peaks) increases by about 0.006, when all other factors remain the same. The intercepts are given by α_i values, which represent the log of the odds of occurrence of at least *i* peaks when the dose level is 1 μM and all other factors are the base level of 0. SE is the standard error for each coefficient, and the *p*-values indicate the statistical significance of each result.

Coefficient	Estimate	SE	*p*-value
β_1 (Effect of Time)	-0.006	0.003	0.036
β_2 (Effect of Area)	0.022	0.003	<0.001
β_1 (Effect of Dose Level 2 μM)	0.024	0.180	0.900
β_1 (Effect of Dose Level 4 μM)	-0.984	0.239	<0.001
β_1 (Effect of Dose Level 8 μM)	-1.190	0.258	<0.001
β_1 (Effect of Dose Level 16 μM)	-1.417	0.487	0.004
α_1	-1.797	0.230	
α_2	-0.298	0.217	
α_3	3.208	0.294	
α_4	6.762	1.053	

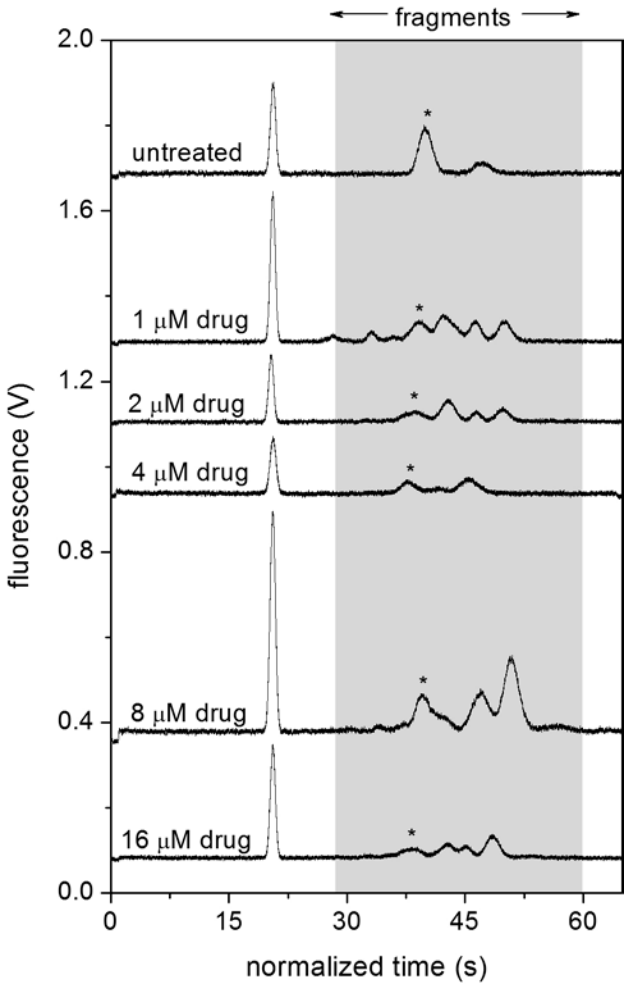

Figure 5. Microchip separations of select ensemble samples run under conditions similar to those on the chemical cytometry device for the traces shown in Figure 3a. Migration times were normalized to the internal standard, carboxyfluorescein, which was the first peak in each electropherogram. The peak for the labeled lysine (K-FAM, *) was identified by standard addition to each sample.

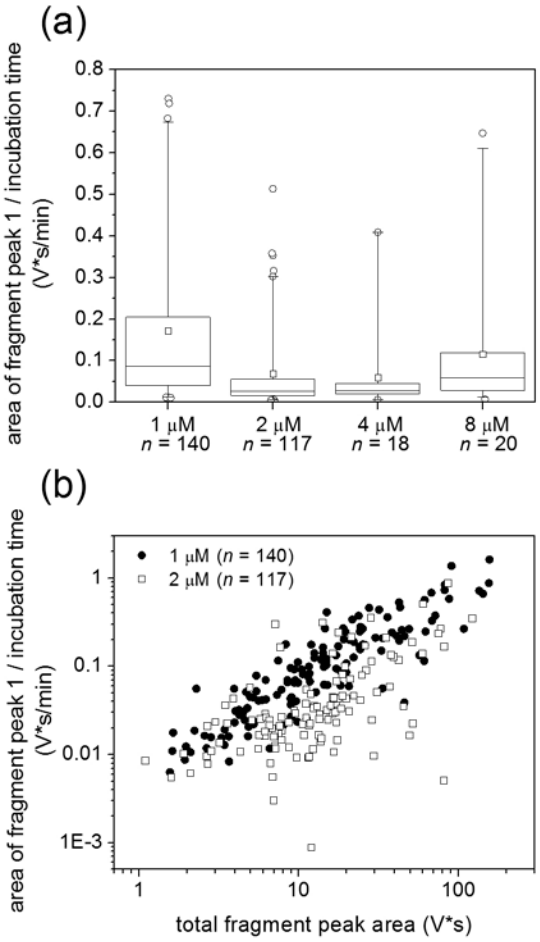

Figure 6. (a) Box plot of the proxy for rate of degradation, calculated from the area of fragment peak 1 divided by the incubation time. The boxes contain the 25th to 75th percentile with a line at the median. The mean value is indicated with an open square. Whiskers show the 5th and 95th percentiles, and outliers are shown as individual points. (b) The average rate proxy as a function of total fragment peak area for cells treated with 1 μM (solid circles) or 2 μM (open squares) Tosedostat. Each data point in this plot represents an individual cell that possessed three fragment peaks. Data points for higher doses are shown in Figure S-3.

Table 3. Results of the adjusted linear regression model.

Coefficient	Estimate	Confidence Interval	*p*-value
β_0 (Intercept)	0.05	(0.044,0.062)	
$\exp(\beta_1)$ (Effect of Area)	1.02	(1.019,1.026)	< 0.01
$\exp(\beta_2)$ (Dose Level 2 μM)	0.41	(0.331,0.521)	< 0.01
$\exp(\beta_3)$ (Dose Level 4 μM)	0.31	(0.196,0.478)	< 0.01
$\exp(\beta_4)$ (Dose Level 8 μM)	0.34	(0.221,0.531)	< 0.01

References

(1) D. Hanahan, R. A. Weinberg, *Cell* **2011**, *144*. 646-674.
(2) L. Ding, et al., *Nature* **2012**, *481*. 506-510.
(3) T. L. Yuan, G. Wulf, L. Burga, L. C. Cantley, *Curr. Biol.* **2011**, *21*. 173-183.
(4) D. Singh, C.-J. Ky, C. Wichaidit, R. Steininger, III, L. Wu, S. Altschuler, *Mol. Syst. Biol.* **2010**, *6*. 369.
(5) M. D. Slack, E. D. Martinez, L. F. Wu, S. J. Altschuler, *Proc. Nat. Acad. Sci. USA* **2008**, *105*. 19306-19311.
(6) M. Greaves, C. C. Maley, *Nature* **2012**, *481*. 306-313.
(7) I. Chiodi, C. Belgiovine, F. Dona, A. I. Scovassi, C. Mondello, *Cancers* **2011**, *3*. 1111-1128.
(8) A. A. Cohen, et al., *Science* **2008**, *322*. 1511-1516.
(9) S. J. Altschuler, L. F. Wu, *Cell* **2010**, *141*. 559-563.
(10) K. E. Gascoigne, S. S. Taylor, *Cancer Cell* **2008**, *14*. 111-122.
(11) M. Niepel, S. L. Spencer, P. K. Sorger, *Curr. Opin. Chem. Biol.* **2009**, *13*. 556-561.
(12) P. O. Krutzik, J. M. Crane, M. R. Clutter, G. P. Nolan, *Nat. Chem. Biol.* **2008**, *4*. 132-142.
(13) M. L. Kovarik, N. L. Allbritton, *Trends Biotechnol.* **2011**, *29*. 222-230.
(14) D. Jiang, C. E. Sims, N. L. Allbritton, *Faraday Discuss.* **2011**, *149*. 187-200.
(15) A. Proctor, Q. Wang, D. S. Lawrence, N. L. Allbritton, *Analyst* **2012**, *137*. 3028-3038.
(16) A. Proctor, Q. Wang, D. S. Lawrence, N. L. Allbritton, *Anal. Chem.* **2012**, *84*. 7195-7202.
(17) A. Zarrine-Afsar, S. N. Krylov, *Anal. Chem.* **2003**, *75*. 3720-3724.
(18) R. M. Phillips, E. Bair, D. S. Lawrence, C. E. Sims, N. L. Allbritton, *Anal. Chem.* **2013**, *85*. 6136-6142.
(19) S. N. Arkhipov, M. Berezovski, J. Jitkova, S. N. Krylov, *Cytom. Part A* **2005**, *63A*. 41-47.
(20) R. B. Brown, J. A. Hewel, A. Emili, J. Audet, *Cytom. Part A* **2010**, *77A*. 347-355.
(21) M. L. Kovarik, P. K. Shah, P. M. Armistead, N. L. Allbritton, *Anal. Chem.* **2013**, *85*. 4991-4997.
(22) X. C. Le, W. Tan, C. H. Scaman, A. Szpacenko, E. Arriaga, Y. Zhang, N. J. Dovichi, O. Hindsgaul, M. M. Palcic, *Glycobiol.* **1999**, *9*. 219-225.
(23) C. D. Whitmore, O. Hindsgaul, M. M. Palcic, R. L. Schnaar, N. J. Dovichi, *Anal. Chem.* **2007**, *79*. 5139-5142.
(24) M. A. McClain, C. T. Culbertson, S. C. Jacobson, N. L. Allbritton, C. E. Sims, J. M. Ramsey, *Anal. Chem.* **2003**, *75*. 5646-5655.
(25) H.-Y. Wang, C. Lu, *Chem. Comm.* **2006**. 3528-3530.
(26) K. S. Phillips, H.-H. Lai, E. Johnson, C. E. Sims, N. L. Allbritton, *Lab Chip* **2011**, *11*. 1333-1341.
(27) H. K. Wu, A. Wheeler, R. N. Zare, *Proc. Nat. Acad. Sci. USA* **2004**, *101*. 12809-12813.
(28) J. Gao, X.-F. Yin, Z.-L. Fang, *Lab Chip* **2004**, *4*. 47-52.
(29) Y. Sun, M. Lu, X.-F. Yin, X.-G. Gong, *J. Chromatogr., A* **2006**, *1135*. 109-114.
(30) F. Xia, W. Jin, X. F. Yin, Z. Fang, *J. Chromatogr., A* **2005**, *1063*. 227-233.
(31) S. Zhao, Y. Huang, Y.-M. Liu, *J. Chromatogr., A* **2009**, *1216*. 6746-6751.
(32) S. Zhao, X. Li, Y.-M. Liu, *Anal. Chem.* **2009**, *81*. 3873-3878.
(33) F. Ye, Y. Huang, Q. Xu, M. Shi, S. Zhao, *Electrophoresis* **2010**, *31*. 1630-1636.

(34) C. X. Xu, M. Wang, X. F. Yin, *Analyst* **2011**, *136*. 3877-3883.
(35) A. J. Dickinson, P. M. Armistead, N. L. Allbritton, *Anal. Chem.* **2013**, *85*. 4797-4805.
(36) E. C. Metto, et al., *Anal. Chem.* **2013**, *85*. 10188-10195.
(37) D. Krige, et al., *Cancer Res.* **2008**, *68*. 6669-6679.
(38) G. M. Dubowchik, M. A. Walker, *Pharmacol. Therapeut.* **1999**, *83*. 67-123.
(39) D. C. Duffy, J. C. McDonald, O. J. A. Schueller, G. M. Whitesides, *Anal. Chem.* **1998**, *70*. 4974-4984.
(40) K. S. Phillips, S. Kottegoda, K. M. Kang, C. E. Sims, N. L. Allbritton, *Anal. Chem.* **2008**, *80*. 9756-9762.
(41) M. L. Kovarik, H.-H. Lai, J. C. Xiong, N. L. Allbritton, *Electrophoresis* **2011**, *32*. 3180-3187.
(42) P. A. Quinto-Su, H.-H. Lai, H. H. Yoon, C. E. Sims, N. L. Allbritton, V. Venugopalan, *Lab Chip* **2008**, *8*. 408-414.
(43) A. Agresti, *Categorical Data Analysis*. 2nd ed.; Wiley-Interscience: Hoboken, NJ, 2002; p 734.
(44) H. M. Coley, in *Cancer Cell Culture*, ed. S. P. Langdon. Humana Press: Totowa, NJ, 2004, vol. 88, pp 267-273.
(45) C. Jenkins, S. Hewamana, D. Krige, C. Pepper, A. K. Burnett, *Leukemia Res.* **2011**, *35*. 677-681.
(46) P. McCullagh, J. A. Nelder, *Generalized Linear Models*. 2nd ed.; Chapman and Hall: 1989; p 532.